Lattice Boltzmann simulation of mass transfer in thermally driven cavity flows

Huidan Yu*

Computer, Computation, and Science Division,
Center for Nonlinear Studies,
Los Alamos National Laboratory, USA
E-mail: hyu@lanl.gov
*Corresponding author

Jinsuo Zhang

Decision Applications Division,
Los Alamos National Laboratory, USA
E-mail: jszhang@lanl.gov

Ning Li

Material Physics and Application Division,
Los Alamos National Laboratory, USA
E-mail: ningli@lanl.gov

Abstract: We study mass transfer in 2D thermally driven cavity using lattice Boltzmann method. Simulations are performed to investigate various effects on enhancement of oxygen mass transfer in lead/lead-bismuth eutectic. It is shown that oxygen transfer is dominated by convection although diffusion plays a role. Comparative studies demonstrate that side-heating and top-cooling configuration is more efficient than side-heating/cooling and oxygen transfers more rapidly in a square than rectangular cavity with same area. This work supplies supportive information for developing active oxygen control technique in experiments to prevent or reduce corrosion in liquid metal cooled nuclear reactors.

Keywords: lattice Boltzmann Method; LBM; Boussinesq equations; thermally driven cavity flow; heat and mass transfer; natural convection.

Reference to this paper should be made as follows: Yu, H., Zhang, J. and Li, N. (2008) 'Lattice Boltzmann simulation of mass transfer in thermally driven cavity flows', *Progress in Computational Fluid Dynamics*, Vol. 8, Nos. 1–4, pp.206–212.

Biographical notes: Huidan Yu is a postdoctoral research associate of Los Alamos National Laboratory, USA. She received her PhD Degrees in Aerospace Engineering from Texas A&M University, USA in 2004 and Physics from Peking University, China, in 2001 successively. Her research interests are on kinetic theory (Boltzmann equation) and hydrodynamics (Navier-stokes equations) based modelling and computation for complex flows including hydrodynamics (incompressible and compressible turbulence), mass/heat transfer, thermodynamics, and reaction kinetics, etc.

Jinsuo Zhang is a staff member at the Los Alamos National Laboratory, USA. He received his PhD in Fluid Mechanics from the Zhejiang University, China, in 2001. His research interests include numerical simulation and modelling of fluid mechanics and material corrosion.

Ning Li is a Project Leader and technical staff member of the Los Alamos National Laboratory, USA. He received a PhD in Physics from the University of California, Santa Barbara, USA, in 1991. He has conducted research in the fields of nonlinear dynamics of pattern formation in fluid systems, advanced separation technologies, thermal hydraulics, coolant technologies and materials for advanced nuclear systems.

1 Introduction

Heat and mass transfer induced by natural convection in cavities are very common in a variety of engineering and environmental applications. Examples include crystal growth (Selver et al., 1998), cooling (Bilgen et al., 1995), glass melting (Sarris et al., 2002), protective oxidisation in lead and lead-bismuth eutectic (Zhang and Li, 2005), etc.

Traditionally, a great deal of complex combined thermal fluid flow problems are solved by the control method based on the finite difference approximation of Navier-Stokes (NS) equations. Numerical tools have been developed by research groups (Marshall et al., 1978; Vahl Davis, 1983; Vahl Davis and Jones, 1983; Le Quéré, 1991; Ismail and Scalon, 2000; Ding et al., 2004).

Lattice Boltzmann Equation (LBE) method (McNamara and Zanetti, 1988) has emerged as an alternative to traditional numerical approaches due to some advantages such as simplicity, parallelisability, and robustness. Extensive applications are found in computation of isothermal incompressible flows (Chen and Doolen, 1998; Luo, 2000; Yu et al., 2003). Nevertheless, the extension of lattice Boltzmann method (LBM) to allow closure at the energy moment level has encountered some difficulties. A critical barrier seems to be the numerical instability occurring when the flow velocity increases. Continued development of thermal LBE models is vital (cf. Lallemand and Luo, 2003 and references therein). Of particular relevance to the present work is to solve Boussinesq equations for natural convection. Recent efforts include benchmark validations (Peng et al., 2003; Zhou et al., 2004; Mezrhab et al., 2004; Shi et al., 2005; Treeck et al., 2006) demonstrating the reliability of these models in simulating heat transfer due to natural convection. To our best knowledge, all reported results are only for heat transfer.

In this work, we intend to study the enhancement of oxygen transfer in lead/lead-bismuth eutectic using LBM. There are strong current interests worldwide in using lead and its alloys (particularly lead-bismuth eutectic) for nuclear coolant applications. Oxygen activity control in lead/lead-bismuth eutectic is of great scientific and technological importance to prevent or reduce corrosion of liquid metal cooled nuclear reactors (Zhang and Li, 2005). We employ the unified thermal LBE model (Shi et al., 2005) that has eliminated the compressibility effect (Guo et al., 2000). This model has been validated in 2D and 3D simulations and is reliable for heat transfer with Boussinesq approximation (Shi et al., 2005; Guo et al., 2002). However, this LBE model only solves velocity and temperature fields for heat transfer. We extend this LBE model for mass transfer by presenting an LBE for concentration field which is coupled with the velocity and temperature fields. We focus on factors which affect the enhancement of oxygen transfer. Simulations of variations in three factors are performed: heating- cooling arrangement, Schmidt (Sc) number, and field Aspect Ratio (AR). Various quantities characterising the mass transfer are computed such as mean and local concentration, mean and local Schwood (Sh) numbers, velocity, etc. Oxygen transfer mechanisms are examined.

The remainder of this paper is organised as follows. Section 2 introduces the mathematical formulation and the LBE model. Section 3 presents the numerical results. Finally Section 4 provides a short summary and concludes the paper.

2 Lattice Boltzmann equations

The problem being considered is a two-dimensional Boussinesq flow in a cavity with height H(z direction) and width L (x direction). Cavity aspect ratio is defined as $AR = L/H$. Boussinesq approximation assumes that the fluid properties such as density (ρ), viscosity (ν), mass diffusivity (D), and thermal diffusivity (κ) are constants except in the body force term where ρ is assumed to be a linear function of the temperature: $\rho = \rho_0[1 - \beta(T - T_0)]$ with ρ_0, T_0 the average density and temperature in the field and β the coefficient of thermal expansion. It is noted that in our practical problem the variation of the mass concentration is much smaller than the temperature change, thus, the influence of the concentration variation on density is neglected. A dimensionless scaling uses height H, velocity $\kappa\sqrt{Ra}/H$, pressure $\rho\kappa^2 Ra/H^2$, time $H^2/(\kappa\sqrt{Ra})$, temperature ΔT $(= T_h - T_l)$, and concentration $C_{\max}$ to normalise the respective quantities. Here T_h and T_l are the heating and cooling temperatures at the boundaries and $C_{\max}$ is the supply mass concentration which is assumed to be a constant. The Rayleigh number is $Ra = (g\beta\Delta T H^3)/(\nu\kappa)$.

The dimensionless Boussinesq equations including velocity, temperature, and concentration fields thus read

$$\nabla \cdot \vec{u} = 0, \tag{1a}$$

$$\frac{\partial \vec{u}}{\partial t} + \vec{u} \cdot \nabla \vec{u} = -\nabla p + \nu_d \nabla^2 \vec{u} + \vec{F}, \tag{1b}$$

$$\frac{\partial \Theta}{\partial t} + \vec{u} \cdot \nabla \Theta = \kappa_d \nabla^2 \Theta, \tag{1c}$$

$$\frac{\partial \Gamma}{\partial t} + \vec{u} \cdot \nabla \Gamma = D_d \nabla^2 \Gamma, \tag{1d}$$

where $\vec{F}$ is the dimensionless body force reflecting gravity, $\nu_d\,(= Pr/\sqrt{Ra})$, $\kappa_d\,(= 1/\sqrt{Ra})$, and $D_d\,(= Pr/(Sc\sqrt{Ra}))$ are dimensionless viscosity, thermal diffusivity, and mass diffusivity respectively. Pr $(= \nu/\kappa)$ is the Prandtl number and Sc $(= \nu/D)$ is the Schmidt number. The body force is computed as $\vec{F} = Pr\Theta\vec{k}$ with $\vec{k}$ the unit vector along the $z-$axis.

The basic LBE consists of two computational steps of particle motion: collision (relaxation) and streaming (advection). The particle distribution function is thermalised locally through a collision process. Streaming to the closest neighbouring sites occurs according to a small set of discrete particle velocities. For the sake of simplicity without losing generality, we adopt the nine-velocity lattice model (D2Q9). The discrete particle velocities are $\vec{e}_\alpha = 0$ for $\alpha = 0, \cos[(\alpha-1)\pi/2]\vec{i} + \sin[(\alpha-1)\pi/2]\vec{k}$ for $\alpha = 1:4$, and $\cos[(\alpha-5)\pi/2 + \pi/4]\vec{i} + \sin[(\alpha-5)\pi/2 + \pi/4]\vec{k}$ for $\alpha = 5:8$.

The LBE for incompressible flow is (Guo et al., 2000):

$$g_\alpha(\vec{x} + c\vec{e}_\alpha\delta_t, t + \delta_t) = g_\alpha(\vec{x}, t) - \frac{1}{\tau_f}[g_\alpha(\vec{x}, t) - g_\alpha^{(eq)}(\vec{x}, t)] + F_\alpha, \tag{2}$$

where g_α $(\alpha = 0, 1, \ldots, 8)$ is the particle distribution function and τ_f is the relaxation time. The corresponding equilibrium distribution function $g_\alpha^{(eq)}$ is defined by

$$g_\alpha^{(eq)} = \lambda_\alpha p + s_\alpha(\vec{u}), \tag{3}$$

where

$$s_\alpha(\vec{u}) = w_\alpha[(c\vec{e}_\alpha \cdot \vec{u})/c_s^2 + (c\vec{e}_\alpha \cdot \vec{u})^2/(2c_s^4) - u^2/(2c_s^2)], \tag{4}$$

with p the pressure fluctuation, weighting factor $\omega_\alpha = 4/9$ $(\alpha = 0)$, $1/9$ $(\alpha = 1:4)$, and $1/36$ $(\alpha = 5:8)$ and parameter $\lambda_\alpha = -5/(3c^2)\,(\alpha = 0), 1/(3c^2)\,(\alpha = 1:4)$, and $1/(12c^2)$ $(\alpha = 5:8)$. The lattice constant $c = \delta_x/\delta_t$ is related to the sound speed of the model as $c = \sqrt{3}c_s$. Discrete body force is computed as (Guo et al., 2002) $F_\alpha = \delta t \chi_\alpha \vec{e}_\alpha \cdot \vec{F}/(2c)$ where $\chi_\alpha = 1$ for $\alpha = 2, 4$ and $\chi_\alpha = 0$ otherwise, which satisfies $\sum_{i=0}^{8} F_\alpha = 0$ and $\sum_{i=1}^{8} F_\alpha c\vec{e}_\alpha = \vec{F}$. The macroscopic flow velocity, pressure, and the dimensionless viscosity are given by $\vec{u} = \sum c\vec{e}_\alpha g_\alpha$, $p = -\lambda_0^{-1}[\sum g_\alpha - g_0 + s_0(\vec{u})]$, and $\nu_d = (\tau_f - 0.5)c\delta x/3$. This LBE model has eliminated the compressibility effect present in other existing LBE models and performs better for incompressible flows (Guo et al., 2000).

The LBEs for temperature and concentration fields are constructed in a same fashion

$$\Theta_\alpha(\vec{x} + c\vec{e}_\alpha\delta_t, t + \delta_t) = \Theta_\alpha(\vec{x}, t) - \frac{1}{\tau_T}[\Theta_\alpha(\vec{x}, t) - \Theta_\alpha^{(eq)}(\vec{x}, t)], \tag{5}$$

and

$$\Gamma_\alpha(\vec{x} + c\vec{e}_\alpha\delta_t, t + \delta_t) = \Gamma_\alpha(\vec{x}, t) - \frac{1}{\tau_C}[\Gamma_\alpha(\vec{x}, t) - \Gamma_\alpha^{(eq)}(\vec{x}, t)], \tag{6}$$

where Θ_α and Γ_α are discrete temperature and concentration in the D2Q9 lattice.

The macroscopic variables of temperature, concentration are $\Theta = \sum \Theta_\alpha$ and $\Gamma = \sum \Gamma_\alpha$, and the dimensionless transport coefficients of thermal diffusivity and mass diffusivity are related to their corresponding relaxation times as $\kappa_d = (\tau_T - 0.5)c\delta x/3$ and $D_d = (\tau_C - 0.5)c\delta x/3$. Notice that relaxation times are related as $\tau_T = (\tau_f - 0.5)/Pr + 0.5$ and $\tau_C = (\tau_f - 0.5)/Sc + 0.5$, the corresponding equilibria $\Theta_\alpha^{(eq)}$ and $\Gamma_\alpha^{(eq)}$ are given by $\Theta_\alpha^{(eq)} = \Theta[\omega_\alpha + s_\alpha(\vec{u})]$ and $\Gamma_\alpha^{(eq)} = \Gamma[\omega_\alpha + s_\alpha(\vec{u})]$.

It is straightforward to prove that LBEs (2), (5) and (6) recover the above dimensionless Boussinesq equations in low Mach number limit using the Chapman-Enskog analysis.

3 Simulations and results

We study oxygen transfer in low Pr $(= 0.0175)$ number liquid lead/lead-bismuth eutectic at $Ra = 3116.3$. Liquid lead or lead-bismuth filled in the cavity is thermally driven by natural convection. Oxygen is supplied from the gas cover at the top and transported into the whole cavity. We define the mean oxygen concentration Γ_m of the whole field, local Sherwood number $Sh(x)$, and mean Sherwood number Sh_m at the gas-liquid interface $(z = 1)$ to characterise the oxygen transfer as $\Gamma_m = \int \Gamma(x, z)\mathrm{d}x\mathrm{d}z / \int\int \mathrm{d}x\mathrm{d}z$, $Sh(x) = \partial\Gamma/\partial z(x, 1)/(1 - \Gamma_m)$, and $Sh_m = \int Sh(x)\mathrm{d}x / \int \mathrm{d}x$.

In what follows, we present three simulations to demonstrate how temperature boundary, Sc number, and cavity AR affect the oxygen transfer in lead/lead-bismuth eutectic. All the instantaneous profiles including velocity and local Sh number are at dimensionless time $t = 1669$.

3.1 Temperature boundary effect

As depicted in Figure 1, we consider two heating-cooling arrangements. In Case 1, the liquid metal is heated at right and cooled at left with adiabatic top cover and bottom wall; while in Case 2, vertical walls are hot and top cover is cool. The bottom wall is adiabatic. We set $Sc = 17.5$ in this simulation.

Figure 1 Two boundary cases simulated for oxygen transfer in lead/lead-bismuth eutectic. Two dots in Case 1 (left) at (0.17, 0.99) and (0.5, 0.01) are oxygen sensors

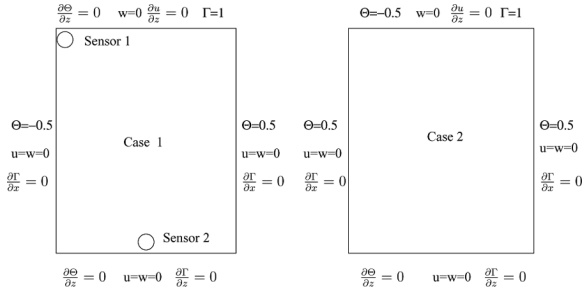

It should be pointed out that although this problem seems to be the same as the one studied using NS-based computation by a group (Ma et al., 2005) including two of the authors of this work, it is indeed different. By using an NS based approach, that work (Ma et al., 2005) only solves the velocity and temperature fields. Mass supply is introduced after the flow becomes steady, which is not a realistic process. Transients are of interest but cannot be studied in the approach. The current LBM approach solves the three fields simultaneously for heat and mass transfer. It is possible to investigate unsteady heat and mass transfer properties. In fact, further simulations focusing on the heat and mass transfer characteristics during the transition from laminar to turbulence are ongoing. In addition, this work strives to analyse the effect of temperature boundary on the mechanisms of oxygen transfer.

We set $u = w = \Theta = p = \Gamma = 0$ everywhere initially in the domain. Boundary conditions of the three related fields are given in Figure 1. We assume equilibrium distributions at the boundaries for all three fields although boundary condition of higher order accuracy (Guo et al., 2000) is

available if needed. Parameters τ_f, T_h, and T_l are set to 0.556, 0.5, and -0.5. Grid size for a unit length is 130.

Figure 2 shows the time evolution of the mean oxygen concentration in the whole field for the two cases. The mean oxygen concentration grows monotonically indicating that oxygen is transferred from the cover gas supply to the whole domain. It can be seen clearly that the mean oxygen concentration grows faster in Case 2 than Case 1 implying that Case 2 has better enhancement of oxygen transfer than Case 1. In order to better understand the oxygen transfer mechanism, we study some pertinent factors.

Figure 2 Evolution of the mean oxygen concentration. Case 1: open triangles and Case 2: solid triangles

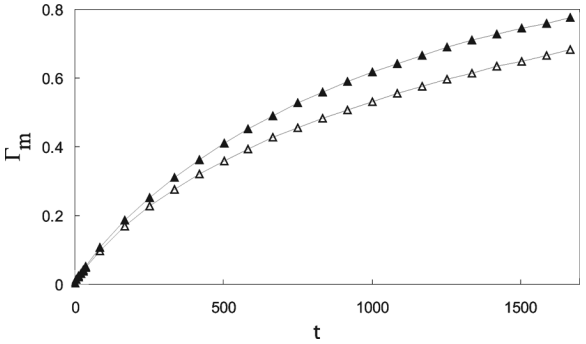

Figure 3 shows the oxygen concentration contours at three times at $t = 83$, 250, and 1669 from left to right. Case 1 is at the top and Case 2 the bottom. The instantaneous flow structures of the two cases corresponding to the latest time in Figure 3 are plotted in Figure 4. The contour patterns and flow structures of the two cases are quite different. In Case 1, oxygen is first driven to the upper-left corner at the cool side wall where oxygen attains the high concentration (Fig. 3(a)). Oxygen is then transferred, in a counterclockwise path, down along the cool wall and across the bottom and up along the hot wall on the right. This transfer forms a nearly circular distribution of oxygen (Fig. 3(b)) with oxygen concentration decreasing toward the centre (Fig. 3(c)). In Case 2, oxygen is first transferred vertically down the mid-line from the gas cover and then splits into two streams at the bottom wall toward two opposite directions and both streams go up along the hot walls (Fig. 3(d)). As a result, two oval distribution regions, counterclockwise left and clockwise right, are formed (Figs. 3(e) and (f)). In both cases, the late time concentration contours are in the same patterns as the flow structures, seen in Figure 4, demonstrating that free convection dominates the oxygen transfer.

The instantaneous velocity profiles of u and w components at the gas-liquid interface show the quantitative difference of oxygen transfer of two cases. As shown in Figure 5(a), in Case 1 there is only one peak velocity (one vortex) while in Case 2 there are two peaks in opposite directions (two vortices). Meanwhile, the u-velocity is larger in Case 2 than in Case 1. The peak value of the former is about two times larger than that of the latter. It is speculated that the stronger stirring occurs in Case 2 than Case 1, leading to more efficient oxygen transfer. Figure 5(b) shows the distribution of w-component along the x direction right beneath the gas-liquid interface at the same time. We see that the oxygen is transferred into the cavity from different regions in the two cases, $x < 0.55$ in Case 1 and $0.3 < x < 0.7$ in Case 2.

Figure 3 Instantaneous oxygen concentration contours for Case 1 (top) and Case 2 (bottom). Time from left to right: (a) and (d): $t = 83$; (b) and (e): $t = 250$; (c) and (f): $t = 1669$. Contour levels (from top to bottom): 0.9, 0.74, 0.58, 0.42, 0.26, 0.1

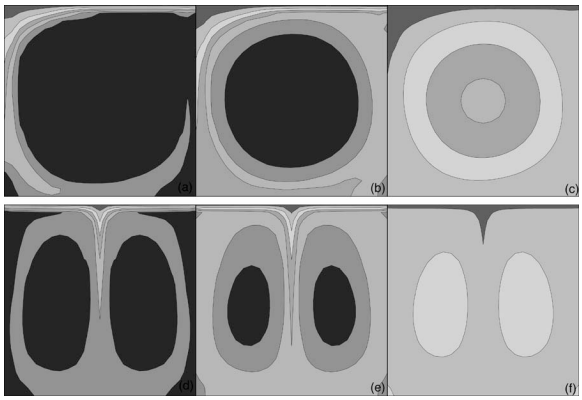

Figure 4 Instantaneous flow structures. (a) Case 1; (b) Case 2. The resolution of the vector fields is five times coarser than that of the corresponding computations for better visualisation

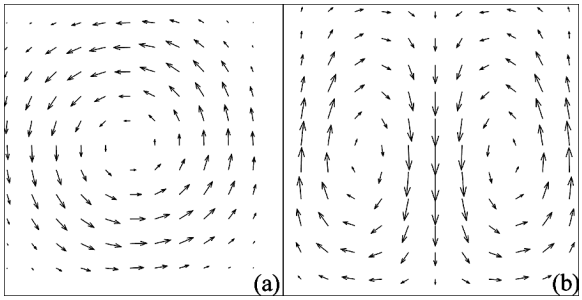

Figure 5 Velocity profiles of u and w components. Case 1: open triangles and Case 2: solid triangles

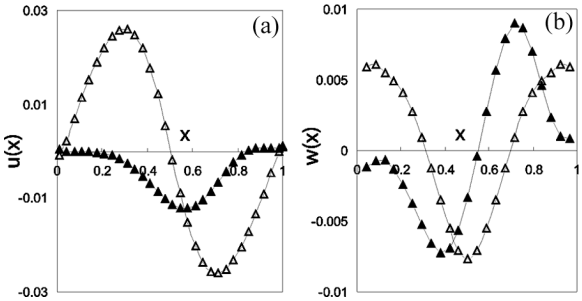

The local Sh distributions and Sh_m evolution of the two cases are also vastly different, as shown in Figure 6. As defined, Sh represents the steepness of oxygen concentration gradient at the gas-liquid interface. Figure 6(a) shows that the oxygen concentration gradient

is small adjacent to the left wall, large in the middle range, and moderate near the right wall; whereas in Case 2 the oxygen segregates in the middle right below the gas cover generating small concentration gradient in the middle but large at both sides. These distributions of local Sh number are consistent with the concentration contours and flow structures in Figures 3 and 4. Figure 6(b) shows the time evolution of Sh_m over the gas-liquid interface. It can be seen that in both cases Sh_m number evolves in the same fashion but the value in Case 2 is larger than that in Case 1 at all times.

Figure 6 (a) The local Sh number profile along the gas-liquid interface and (b) Evolution of the mean Sh number over the gas-liquid interface. Case 1: open triangles and Case 2: solid triangles

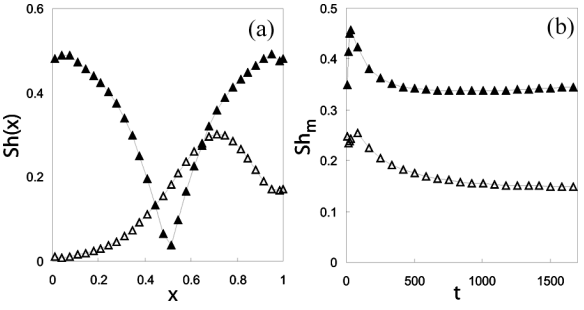

In summary, oxygen transfer is more enhanced in Case 2 than Case 1, which agrees with the results in Ma et al. (2005).

Next, we focus on Case 1 in Figure 1 to study the behaviour of oxygen transfer when Sc number and AR vary. Two oxygen sensors are placed in the field at (0.17, 0.99) and (0.5, 0.01) to measure the development of local oxygen concentration at these two representative locations.

3.2 *Schmidt number effect*

Figure 7(a) shows the time evolutions of the mean oxygen concentration of the field at three different Sc numbers. It is shown that a smaller Sc number corresponds to a faster oxygen concentration growth, since a smaller Sc represents a larger mass diffusivity. This shows that mass diffusion also plays a non-negligible role in the oxygen transfer.

Figure 7 Time evolutions of oxygen concentration at different Sc values. (a) Mean oxygen concentration; (b) local concentration at Sensor 1 (0.17, 0.99) and (c) local concentration at Sensor 2 (0.5, 0.01). $\triangle$: $Sc = 8.75$, $\square$: $Sc = 17.5$, and $\circ$: $Sc = 35$

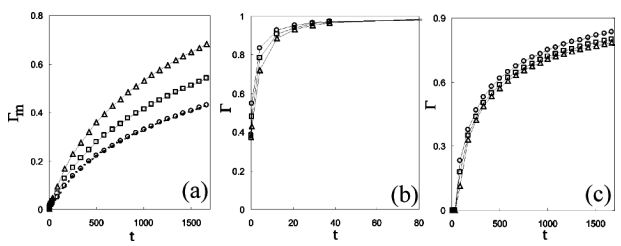

Figure 7(b) shows the local oxygen development at Sensor 1 which is at the corner of the gas-liquid interface and the cool left wall. At this location, local oxygen transfer reaches an equilibrium state very quickly indicating free convection dominates the oxygen transfer. Diffusion contribution is almost invisible. This is closely related to the flow structure as we have described above (Fig. 3(c)). At Sensor 2 which is far away from the gas supply and in the middle of the hot and cool walls, as shown in Figure 7(c), oxygen concentration grows much slower than that at Sensor 1.

3.3 *Aspect ratio effect*

We study the behaviour of oxygen transfer in a square cavity (SC) ($AR = 1$) and a rectangular cavity (RC) ($AR = 0.44$) with the same cavity area to compare the efficiency of oxygen transfer in one cavity over another. The width and length of the RC are selected as $L \times H = (2/3) \times (3/2)$ so that both cavities have the same area. We set $Sc = 8.75$ in this simulation.

Figure 8 shows the time evolutions of the mean oxygen concentration and local oxygen concentrations at two Sensor locations in the two cavities. Both Figures 8(a) and (c) show that the SC (large AR) has much faster oxygen transfer than the RC (small AR). At Sensor 1, shown in Figure 8(b), AR variation does not make a significant difference since the oxygen transfer reaches equilibrium state very quickly at this location in both cavities.

Figure 8 Time evolutions of oxygen concentration, at different Sc values. (a) Mean oxygen concentration; (b) local concentration at Sensor 1 (0.17, 0.99) and (c) local concentration at Sensor 2 (0.5, 0.01). $\triangle$: $AR = 1$, $\circ$: $AR = 0.44$

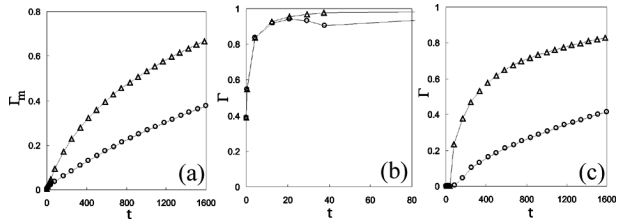

Figure 9 shows the distribution of local Sh number and the time evolution of the corresponding Sh_m value. It is seen that the RC sustains steeper oxygen concentration gradient at the gas-liquid interface than the SC (Fig. 9(a)) and the mean Sh_m is larger in the former than in the latter after a short transition from the time oxygen transfer starts (Fig. 9(b)). This seems to contradict the behaviour of concentration evolution indicated above.

In order to understand this special behaviour, we further examine the flow feature and concentration field in the cavities.

Flow structures in Figure 10(a) and (c) show that in both cavities a single vortex appears. However, in the SC, the convection dominates almost the whole field, while in the RC the vortex only dominates the centre area of the cavity locally. Right beneath the gas cover, oxygen is transferred by free convection in the former but mass

diffusion in the latter, which leads to different oxygen growth rate in the cavities. In the RC, flow is weak in the edge areas at the top and bottom. This difference results in different oxygen transfer patterns (Fig. 10(b) and (d)). In stead of circular distribution, oxygen transfers in an unclosed pattern in the RC, which explains why local Sh is high and increases monotonically from left to right in the RC.

Figure 9 (a) Local Sh number profiles along the gas-liquid interface and (b) evolution of Sh_m number over the gas-liquid interface. $\triangle$: $AR = 1$, $\circ$: $AR = 0.44$

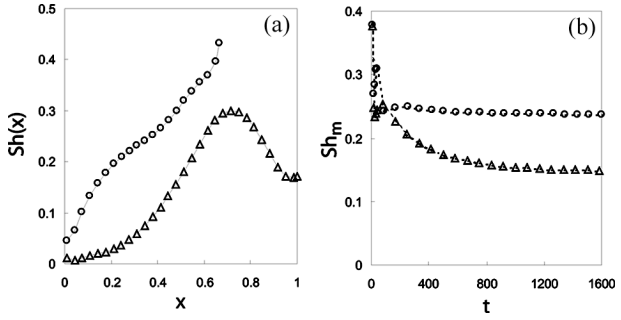

Figure 10 Velocity structures (left) and oxygen concentration contours (right). Top: $AR = 1$; bottom: $AR = 0.44$. The resolution of the vector fields is five times coarser than that of the corresponding computations for better visualisation

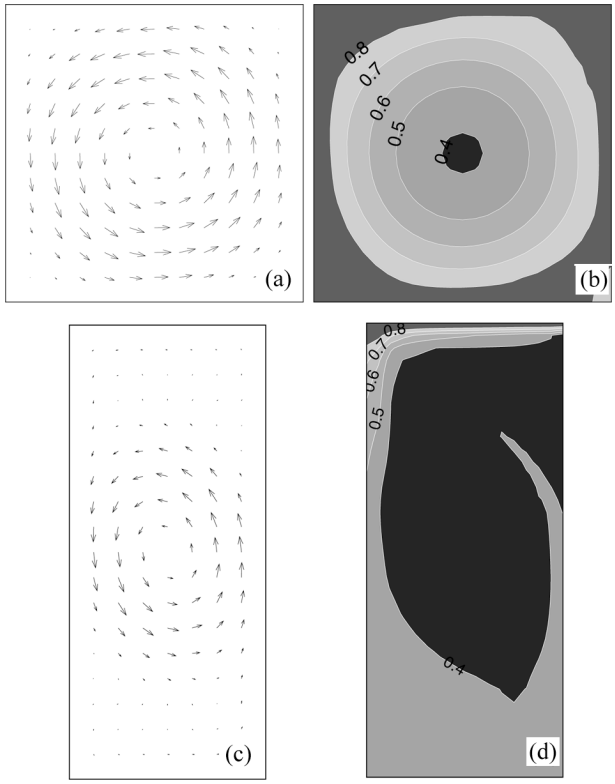

The velocity profiles of u and w components, plotted in Figure 11, show the local flow feature right beneath the gas cover. Although the velocity components have similar distributions, the value are much larger in the SC than in the RC. Besides, the range which allows oxygen transfer into the cavity, $w < 0$, is much wider and the flux is much bigger in the SC than in the RC. Both factors contribute to a faster oxygen transfer in the SC.

Figure 11 Velocity profiles of u and w components along x direction beneath the gas-liquid interface. $\triangle$: $AR = 1$, $\circ$: $AR = 0.44$

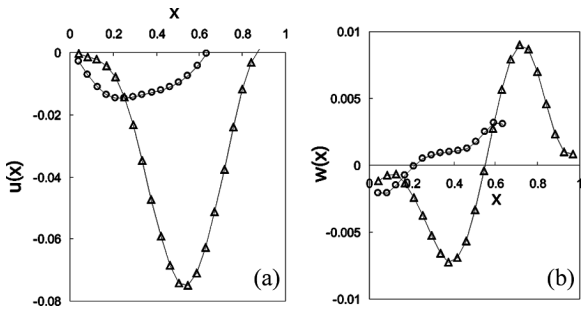

4 Conclusion and discussion

In this work, we simulate oxygen transfer in lead/lead-bismuth eutectic. We focus on the factors which enhance oxygen transfer through varying temperature boundary condition, cavity geometry, and Schmidt number. Our main findings are as follows:

1 The enhancement of oxygen transfer is mainly dominated by convection although mass diffusion does play a role.

2 Side heating and upper cooling arrangement is more effective for oxygen transfer than heating and cooling at both sides, which is in good agreement with results from a numerical calculation based on NS equations (Ma et al., 2005). This is due to the different mass transfer mechanisms in the two arrangements.

3 Square cavity ($AR = 1$) enhances oxygen transfer more than rectangular one ($AR = 0.44$) having the same cavity area. The transfer mechanism together with the flow feature are as follows: in the SC, convection dominates almost the entire area; whereas in the RC, the convection occurs in the centre area and oxygen is transferred into the cavity from the cover gas mostly via diffusion.

This work will provide useful information for active oxygen control technique in experiments. Based on this work, more complex and realistic heat/mass transfer study is being done such as transition of laminar flow to turbulence at higher Ra number, mass transfer with chemical reaction, etc. Important results will be presented in the near future.

Acknowledgement

H. Yu wish to thank Dr. Zhaoli Guo and Professor Baochang Shi for valuable communications. This work was supported by the US DOE Advanced Fuel Cycle Initiative.

References

Bilgen, E., Wang, X., Vasseur, P., Meng, F. and Robillard, L. (1995) 'On the periodic conditions to simulate mixed convection heat transfer in horizontal channels', *Numer. Heat Transfer, Part A*, Vol. 27, pp.461–472.

Chen, S. and Doolen, G.D. (1998) 'Lattice Boltzmann method for fluid flows', *Annu. Rev. Fluid Mech.*, Vol. 30, pp.329.

Ding, H., Shu, C., Yeo, K.S. and Xu, D. (2004) 'Development of least-square-based two-dimensional finite-difference schemes and their application to simulate natural convection in a cavity', *Compu. Fluids*, Vol. 33, pp.137–154.

Guo, Z.L., Shi, B.C. and Wang, N.C. (2000) 'Lattice BGK model for incompressible Navier-Stokes equation', *J. Comp. Phys.*, Vol. 165, pp.288–306.

Guo, Z.L., Shi, B.C. and Zheng, C.G. (2002) 'A coupled lattice BGK model for the Boussinesq equations', *Int. J. Numer. Meth. Fluids*, Vol. 39, pp.325–342.

Ismail, K.A.R. and Scalon, V.L. (2000) 'A finite element free convect model for the side wall heated cavity', *Int. J. Heat Mass Trans.*, Vol. 43, pp.1373–1389.

Lallemand, P. and Luo, L-S. (2003) 'Theory of the lattice Boltzmann method: Acoustic and thermal properties in two and three dimensions', *Phys. Rev. E*, Vol. 68, p.036706.

Le Quéré, P. (1991) 'Accurate solutions to the square thermally driven cavity at high Rayleigh number', *Computers Fluids*, Vol. 20, pp.29–41.

Luo, L-S. (2000) 'The lattice-gas and lattice Boltzmann methods: past, present and future', *Proc. Int. Conf. Applied CFD*, Oct. 17–20, 2000, Beijing, edited by J-H. Wu and Z-J. Zhu, pp.52. (Available at http://research.nianet.org/ luo/nonjournal-pubs.html)

Ma, J., Guo, P., Zhang, J., Li, N. and Fu, B.M. (2005) 'Enhancement of oxygen transfer in liquid lead and lead-bismuth eutectic by natural convection', *Int. J. Heat Mass Trans.*, Vol. 48, pp.2601–2612.

Marshall, R., Heinrich, J. and Zienkiewicz, O. (1978) 'Natural convection in a square enclosure by a finite-element, penalty function method using promitive fluid variables', *Num. Heat Transfer*, Vol. 1, pp.331–349.

McNamara, G.R. and Zanetti, G. (1988) 'Use of the Boltzmann equation to simulate lattice-gas automata', *Phys. Rev. Lett.*, Vol. 61, pp.2332.

Mezrhab, A., Bouzidi, M. and Lallemand, P. (2004) 'Hybrid lattice-Boltzmann finite-difference simulation of convective flows', *Comp. and Fluids*, Vol. 33, pp.623–641.

Peng, Y., Shu, C. and Chew, Y.T. (2003) 'Simplified thermal lattice Boltzmann model for incompressible thermal flows', *Phys. Rev. E*, Vol. 68, p.026701.

Sarris, I.E., Lekakis, I. and Vlachos, N.S. (2002) 'Natural convection in a 2D enclosure with sinusoidal upper wall temperature', *Numer. Heat Transfer, Part A*, Vol. 42, pp.513–530.

Selver, R., Kamotani, Y. and Ostrach, S. (1998) 'Natural convection of a liquid metal in vertical circular cylinders heated locally from the side' , *J. Heat Transfer*, Vol. 120, pp.108–114.

Shi, B., He, N. and Wang, N. (2005) 'A unified thermal lattice BGK model for Boussinesq equations', *Prog. Comput. Fluid Dynam.*, Vol. 5, pp.50–64.

Treeck, C., Rank, E., Krafczyk, M., Tolke, J. and Nachtwey, B. (2006) 'Extension of a hybrid thermal LBE scheme for large-eddy simulations of turbulent convection flows', *Comp. and Fluids*, Vol. 35, pp.863–871.

Vahl Davis, G. (1983) 'Natural convection of air in a square cavity: a bench mark numerical solution', *Int. J. Num. Meth. Fluids*, Vol. 3, pp.249–264.

Vahl Davis, G. and Jones, I. (1983) 'Natural convection in a square cavity: a comparison exercise', *Int. J. Num. Meth. Fluids*, Vol. 3, pp.227–248.

Yu, D., Mei, R., Luo, L-S. and Shyy, W. (2003) 'Viscous flow computations with the method of lattice Boltzmann equation', *Prog. Aerospace Sci.*, Vol. 39, pp.329.

Zhang, J. and Li, N. (2005) 'Oxidation mechanism of steels in liquid-lead alloys', *Oxid. Metals*, Vol. 63, pp.353–379.

Zhou, Y., Zhang, R., Staroselsky, I., and Chen, H. (2004) 'Numerical simulation of laminar and turbulent buoyancy-driven flows using a lattice Boltzmann based algorithm', *Int. J. Heat Mass Trans.*, Vol. 47, pp.4869–4879.